Journal of Theoretical and Applied Mechanics, Sofia, Vol.55 (2025) pp. 460-474
FLUID MECHANICS

LONGITUDINAL RIBS EFFECT ON THE ENHANCEMENT OF HEAT TRANSFER IN TAYLOR-COUETTE-POISEUILLE FLOW

AHMED DAIMALLAH[1‡], MOHAMED LEBBI[2], LYES BOUTINA[2]

[1]*LEMI, Faculty of Technology, University M'hamed Bougara of Boumerdes, Avenue de l'indépendance 35000 Boumerdes, Algeria*

[2]*Unité de Recherche Appliquée en Energies Renouvelables URAER, Centre de Développement des Energies Renouvelables, CDER, 47133 Ghardaïa, Algeria*

[Received: 10 June 2025. Accepted: 8 December 2025]

doi: https://doi.org/10.55787/jtams.25.55.4.460

ABSTRACT: In this study, a three-dimensional simulation was conducted to examine the effect of rib integration on the heat transfer characteristics in Taylor-Couette-Poiseuille flow (TCPF). The ribs are fixed to the periphery of the inner cylinder of the system studied. Three cases were analyzed: 4, 8, and 16 ribs. Initially, the study considers purely axial flow with a stationary inner cylinder, while the next phase evaluates the combined influence of axial flow and cylinder rotation. The findings reveal that the configuration with four ribs achieves the most significant heat transfer improvement, with an increase of up to 312% at higher Re_{eff} values and approximately 103.6% at lower Re_{eff} values.

KEY WORDS: Finite volume method, Taylor-Couette-Poiseuille flow, ribbed inner cylinder, heat transfer.

NOMENCLATURE

r, ϕ, z	Radial, azimuthal and axial coordinate [m]	Re_z	Axial Reynolds number [-]
Ω_1, Ω_2	Inner, Outer rotational velocity [rad/s]	Re_{eff}	Effective Reynolds number [-]
R_1, R_2	Inner, Outer cylinder radius [m]	Re_r	Rotational Reynolds number [-]
T_1, T_2	Inner, outer cylinder temperature [K]	Gr	Grashof number [-]
T_b	Fluid bulk temperature [K]	Fr	Froude number [-]
T_w	Wall temperature [K]	Pr	Prandtl number [-]
θ	Dimensionless temperature [-]	$\overline{NU}$	Average Nusselt number [-]
u, v, w	Radial, azimuthal and axial velocity component	Γ	Aspect ratio [-]
V_z	Axial velocity [m/s]	η	Radius ratio [-]
Δ	Laplacian operator	ρ	Fluid density [kgm^{-3}]

1 INTRODUCTION

The flow between coaxial cylinders became a prone of a continuous scientific interest [1–5], since the pioneering finding of Taylor [6] in 1923, where the existence of

‡Corresponding author e-mail: a.daimallah@univ-boumerdes.dz

the axial wave is revealed. This type of flow is found in various engineering applications, among them we mention rotating membrane filters [7], water treatment [8], rotating heat pipes [9], food engineering [10,11] and medicinal applications [12–14]. Diprima [1] and Schandrasekhar [2] are the first who interested in Taylor-Couette (TC) problem combining an axial flow for a small configuration. Later, Hasoon and Martin [15] extended their study for a relatively large gap. The found a stabilizing effect of the system with axial flow. Their results were confirmed experimentally by Snyder [16]. Lee and Lueptow [17] controlled scale formation in reverse osmosis by means of rotating membranes. Their results indicated that this controlling process significantly contributed to reduce membrane fouling due to scale formation comparatively to non-rotating reverse osmosis. It is concluded that increasing the rotating speed resulted in significant anti-fouling effect because of the increased shear and strengthened vortices. Daimallah et al. [18] analyzed the effect of the concentration of particles and the aspect ratio on the structure of the flow and vortex shape in Taylor-Dean system.By using polarographic method, Kristiawan et al. [19] conducted experimental measurement of both shear rates axial and azimuthal at the outer cylinder of the TCPF. Belkadi et al. [20] investigated numerically the influence of axial flow on the stability Taylor vortex flow. Their results indicated that axial flow delays the primary instability appearance. Recently, Daimallah et al. [21] examined the effect of the modification of the form of the inner cylinder endwall on the Taylor-Couette flow stability. They found that the development of Ekman cells and the onset of vortex of Taylor are delayed for case with two-hemispherical endwalls. Jeng et al. [22] analyzed experimentally the heat transfer in the TCPF system in the presence of axial ribs placed on the rotating inner cylinder. They found that the presence of cavities on the ribs is better to cool the rotating machinery components. Bouafia et al. [23] studied experimentally the convective heat transfer in the gap between coaxial cylinders with and without axial flow. The obtained results for the case with axial flow indicated that the configuration of smooth air gap is better for heat transfer at the rotating cylinder. Lee and al. [24] investigated experimentally the presence of axial wall slits in TC flow system using the technique DPIV. Their results indicated that the axial wall slits accelerate the transition laminar-turbulent. Lee and Minkowycs [25] studied heat transfer characteristics between short coaxial cylinders in presence of axially slit wall. They applied the naphthalene sublimation technique. Their results show qualitative information regarding heat transfer. Liu et al. [26,27] analyzed the stability of TC flow with axially wall slit and temperature gradient. They obtained that the models with larger number of slits affect the flow stability and accelerate the transition process. Chaieb et al. [28] conducted numerical investigation on mixed convection heat transfer in horizontal Taylor-Couette flow. They found that the convection modes affect the appearance of Ekman cells and Taylor vortex and an improvement of heat transfer.

The present work aims to analyze, by numerical simulation, the influence of longitudinal ribs placed on the rotating inner cylinder on the heat transfer of TCPF system. We analyze cases with 4, 8 and 16 ribs. First, we conduct a study for axial flow without rotating the inner cylinder. Secondly, the investigation is extended to the combination between axial flow and rotating inner cylinder. Gambit is used to create the geometry and generate mesh and Ansys Fluent to solve the governing equations.

2 Computational Methodology

2.1 Physical model

Figure 1 depicts the sketch of the flow system and the configuration of the studied cases. The geometrical dimensions of the flow system physical conditions are selected from the work of [22]. The flow system is made up of two coaxial cylinders of radii $R_1 = 0.06$ m and $R_2 = 0.067$ m maintained respectively at temperature T_1 and T_2. The aspect ratio $\Gamma = 17.14$ and the radius ratio $\eta = 0.9$. The fluid contained between cylinders is Newtonian.

2.2 Fundamental equations of the system

The equations that describe the flow are given in cylindrical coordinates (r, ϕ, z):

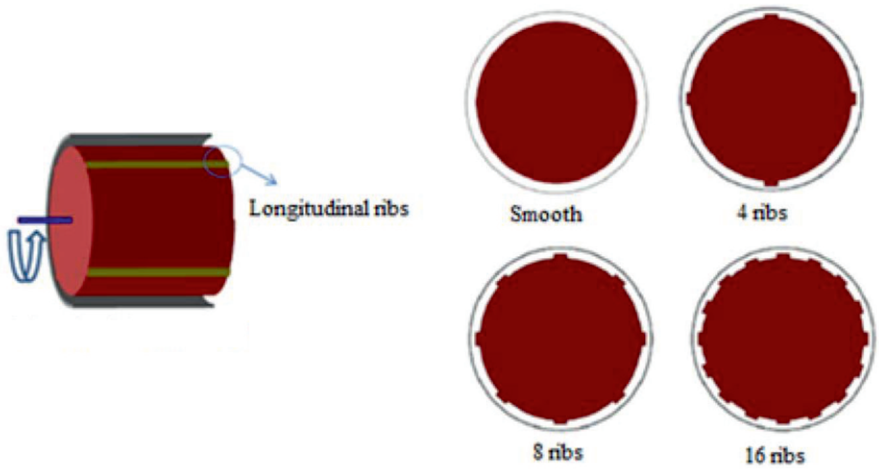

(a) (b)

Fig. 1. Physical model: (a) Sketch of the geometry; (b) several studied configurations.

Continuity equation

(1) $$\frac{1}{r}\frac{\partial(ru)}{\partial r}+\frac{1}{r}\frac{\partial v}{\partial \varphi}+\frac{\partial w}{\partial z}=0\,;$$

Momentum equations

(2) $$\left[u\frac{\partial u}{\partial r}+\frac{v}{r}\frac{\partial u}{\partial \varphi}+w\frac{\partial u}{\partial z}-\left(1-GrFr^2\theta\right)\frac{v^2}{r}\right] = -\frac{\partial p}{\partial r}+\frac{1}{Re_z}\left[\left(\Delta-\frac{1}{r^2}\right)u-\frac{2}{r^2}\frac{\partial v}{\partial \varphi}\right],$$

(3) $$\left[u\frac{\partial v}{\partial r}+\frac{v}{r}\frac{\partial v}{\partial \varphi}+w\frac{\partial v}{\partial z}+\frac{uv}{r}\right]=-\frac{1}{r}\frac{\partial p}{\partial r}+\frac{1}{Re_z}\left[\left(\Delta-\frac{1}{r^2}\right)v-\frac{2}{r^2}\frac{\partial u}{\partial \varphi}\right],$$

(4) $$\left[u\frac{\partial w}{\partial r}+\frac{v}{r}\frac{\partial w}{\partial \varphi}+w\frac{\partial w}{\partial z}\right]=-\frac{\partial p}{\partial r}+\frac{1}{Re_z}\Delta w+\frac{Gr}{Re_z^2}\theta\,;$$

Energy equation

(5) $$\left[u\frac{\partial \theta}{\partial r}+\frac{v}{r}\frac{\partial \theta}{\partial \varphi}+w\frac{\partial \theta}{\partial z}\right]=\frac{1}{\mathrm{Pr}\,Re_z}\Delta\theta\,,$$

where

(6) $$\Delta=\frac{\partial^2}{\partial r^2}+\frac{1}{r}\frac{\partial}{\partial r}+\frac{1}{r^2}\frac{\partial^2}{\partial \varphi^2}+\frac{\partial^2}{\partial z^2}$$

is the Laplacian operator.

The flow control parameters are as follow:

Grashof number

(7) $$Gr=\frac{g\beta\Delta T Dh^3\rho^2}{\mu^2}\,;$$

Axial Reynolds number

(8) $$Re_z=\frac{\rho V_z\left(R_2-R_1\right)}{\mu}\,;$$

Rotational Reynolds number

(9) $$Re_r=\frac{\rho\left(\Omega_1 R_1\right)\left(R_2-R_1\right)}{\mu}\,;$$

Effective velocity

(10) $$V_e = \left[V_z^2 + (\Omega_1 R_1)^2\right]^{0.5} ;$$

Effective Reynolds number

(11) $$Re_{eff} = \frac{\rho V_e \left(R_2 - R_1\right)}{\mu} ;$$

Local Nusselt number

(12) $$Nu = \frac{q \left(R_2 - R_1\right)}{\left(T_w - T_b\right) k} ;$$

Average Nusselt number

(13) $$\overline{Nu} = \frac{\left(\sum_{i=1}^{n} \left(Nu \Delta z\right)_i\right)}{L} ;$$

Froude number

(14) $$Fr = \frac{V_e^2}{g \left(R_2 - R_1\right)} .$$

2.3 Boundary conditions

The following boundary conditions are applied to close the system of governing equations:

2.3.1 Hydrodynamic boundary conditions

- *Inner cylinder wall* (at $r = R_1$, $0 < z < H$):
  First case (purely axial flow): $V_1 = R_1\omega = 0$;
  Second case (rotating inner cylinder): $V_1 = R_1\omega > 0$.

- *Outer cylinder wall* (at $r = R_2$, $0 < z < H$):
  No-slip, stationary wall for both cases. $V_2 = R_2\omega = 0$.

- *Inlet*: A uniform axial velocity ($V_z = U_m$) profile is specified for both cases, corresponding to the axial Reynolds number (Re_z).

- *Outlet*: A pressure-outlet condition with gauge pressure set to zero is applied.

2.3.2 Thermal Boundary Conditions

A constant temperature difference is maintained across the annulus:

- *Inner cylinder wall* (at $r = R_1$, $0 < z < H$):
  Constant wall temperature, $T = T_1 = 310$ K.

- *Outer cylinder wall* (at $r = R_2$, $0 < z < H$):
  Constant wall temperature, $T = T_2 = 300$ K, where $T_1 > T_2$ for heating from the inner cylinder.

- *Inlet*: The fluid enters at a constant temperature equal to the outer cylinder temperature $T_{\text{inlet}} = T_2$.

- *Outlet*: $\dfrac{\partial T}{\partial z} = 0$. A zero-diffusive-flux condition for temperature is applied, implying a fully developed thermal field at the exit.

3 Numerical Procedure

3.1 Numerical technique

Numerical simulations are implemented using Ansys Fluent 14.0 which applied the Finite Volume Method [29]. The pressure-velocity coupling is treated by applying the SIMPLE algorithm. The convective terms in the momentum equations are discretized using a third-order scheme. By using Gambit 3.3.16, the 3-D physical model and meshes were created.

Given that the maximum effective Reynolds number (Re_{eff}) in this study is 600, which corresponds to a laminar flow regime for this geometry, the simulations were conducted by directly solving the laminar governing equations (1)–(5) without employing a turbulence model.

A mesh independence study was conducted to ensure the accuracy of the numerical results. Figure 2 shows the variation of the average Nusselt number versus axial Reynolds number, for different grid cells numbers. As observed, the value of average Nusselt number converges as the mesh density increases. The selected mesh configuration ($18 \times 154 \times 231 \approx 640,000$ cells) lies well within this converged region, ensuring that the results are independent of further grid refinement. This mesh was therefore adopted for all subsequent simulations to optimize computational cost and accuracy.

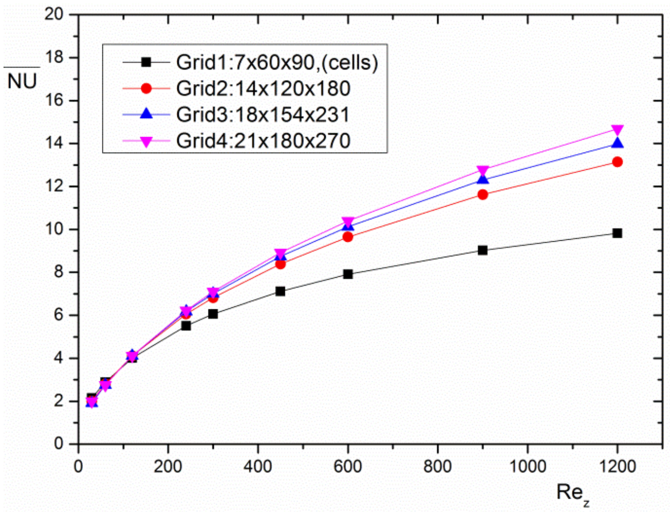

Fig. 2. Evolution of average Nusselt number versus axial Reynolds number.

3.2 Validation model

The validation of numerical model employed in this investigation, has been done by comparison of the obtained numerical results to results of Carpenter et al. [30] for smooth cylinder and also to experimental results of Jeng et al. [22] for a cylinder with 4 ribs as shown in Fig. 3.

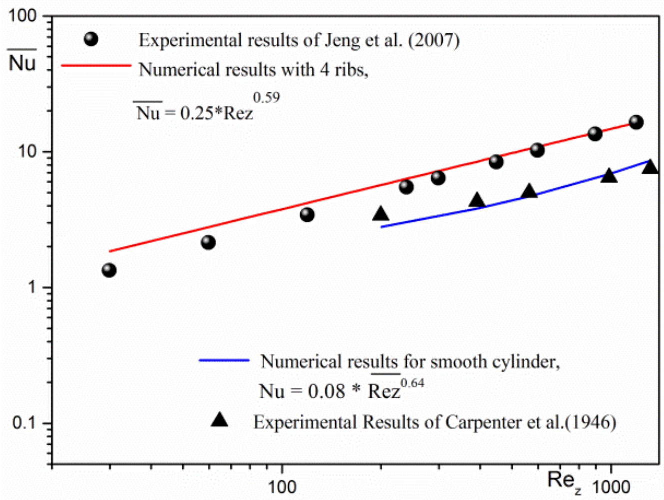

Fig. 3. Average Nusselt number ($\overline{Nu}$) versus axial Reynolds number (Re_z).

A quantitative analysis of the deviation between the present numerical results and the benchmark experimental data was performed. For the smooth cylinder case, the average absolute percentage error was 10.14%. While for the 4-ribbed cylinder case, the error was 9.85% across the Reynolds number range from 30 to 1200. The obtained results show a good agreement with the results of Carpenter et al. [30] and Jeng et al. [22].

4 Results and Discussion

The thermo-hydrodynamic behavior of the flow is analyzed both with and without the rotation of the inner cylinder. Initially, the study examines the TCPF system with a stationary inner cylinder. Subsequently, the impact of the inner cylinder's rotation on the flow dynamics and heat transfer characteristics is investigated.

4.1 Thermo-hydrodynamic flow behaviour for stationary inner cylinder

4.1.1 Axial Reynolds number effects on the axial velocity contours

Figure 4 illustrates the evolution of velocity contours within the gap for different axial Reynolds numbers, comparing a smooth inner cylinder to a ribbed inner cylinder with four ribs. The results indicate that an increase in Re_z leads to a rise in axial velocity within the gap between the cylinders. Additionally, as Re_z increases, noticeable changes occur in the shape of the axial velocity contours for both configurations, with and without ribs.

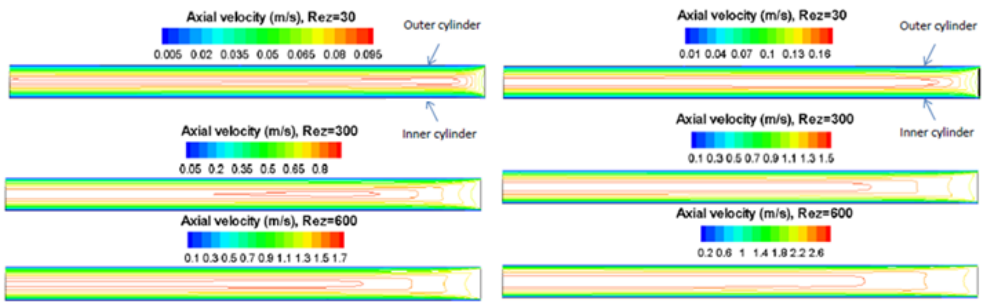

(a) (b)

Fig. 4. Velocity contours development in the meridional plane (r, z) of annular space for: (a) smooth inner cylinder; (b) ribbed inner cylinder with 4 ribs.

4.1.2 Axial Reynolds number effects on the development of temperature contours

Figure 5 illustrates the evolution of temperature contours within the annular region for different Re_z values. The findings indicate that, for both examined cases, the peak temperature in the annular space declines as Re_z increases.

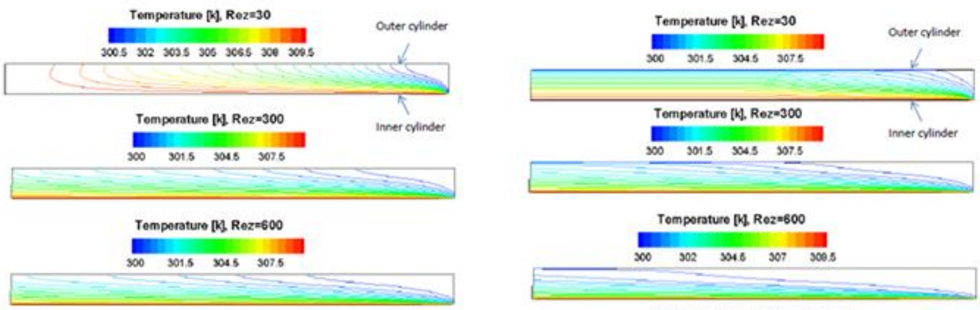

(a) (b)

Fig. 5. Development of temperature contours in the meridional plane (r, z) of the annular space for: (a) smooth inner cylinder; (b) ribbed inner cylinder with 4 ribs.

4.1.3 Axial Reynolds number effects on the variation of temperature field

Figure 6 presents the temperature distribution along the radial direction (at $Z = L/2$) for different axial Reynolds numbers. The results reveal that temperature decreases

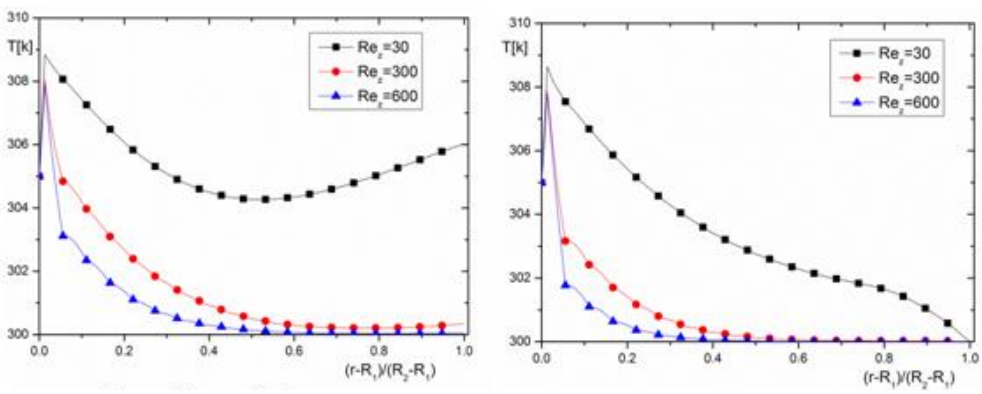

(a) (b)

Fig. 6. Evolution of temperature in the radial direction (at $Z = L/2$ for: (a) smooth inner cylinder; (b) ribbed inner cylinder with 4 ribs.

within the annular space as Re_z increases. This trend can be attributed to the rise in mass flow rate associated with the increase in Re_z.

4.1.4 Axial Reynolds number effects on the average Nusselt number

Figure 7 illustrates the variation of the average Nusselt number ($\overline{Nu}$) as a function of the axial Reynolds number. The results demonstrate that ($\overline{Nu}$) is influenced by the number of ribs attached to the inner cylinder. Specifically, an increase in of $\overline{Nu}$ approximately 29% for $Re_z = 600$ and 59% for $Re_z = 30$ is observed in the configuration with four ribs. These findings indicate that the four-ribs configuration is the most effective in enhancing $\overline{Nu}$ for a stationary inner cylinder.

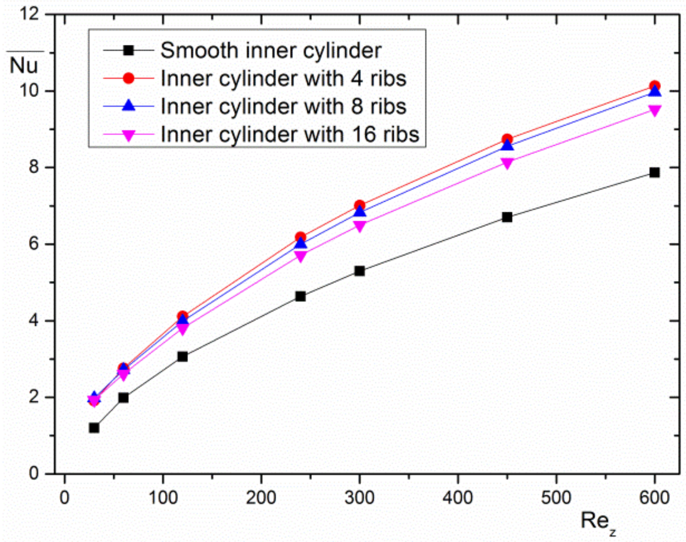

Fig. 7. Average Nusselt number variation ($\overline{Nu}$) versus axial Reynolds number (Re_z) for various numbers of ribs.

4.2 Thermo-hydrodynamic flow behaviour for rotating inner cylinder

4.2.1 Effective Reynolds number effects on the axial velocity contours

Figure 8 shows the evolution of axial velocity contours in the meridian plane (r, z) of the annular space between two coaxial cylinders, for both the smooth inner cylinder and the ribbed inner cylinder with 4 ribs, across various effective Reynolds numbers

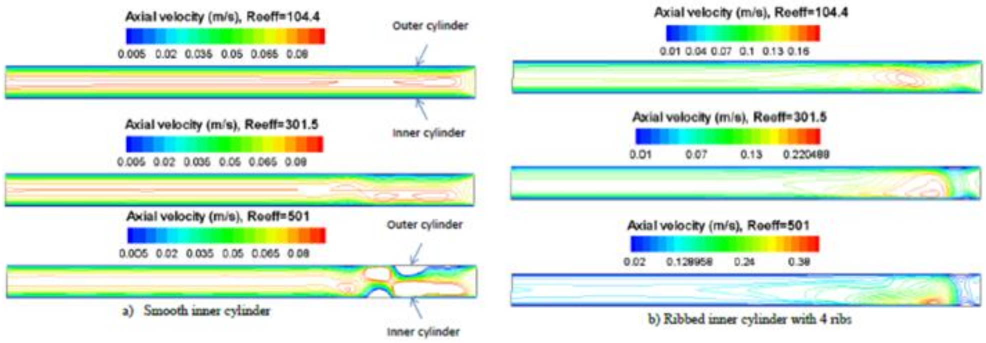

(a) (b)

Fig. 8. Development of axial velocity contours in the meridional plane (r, z) for: (a) smooth inner cylinder; (b) ribbed inner cylinder with 4 ribs.

Re_{eff}. In the case of the smooth inner cylinder, an increase in Re_{eff} leads to the formation of Taylor vortices. However, these vortices vanish when the inner cylinder is ribbed with 4 ribs.

4.2.2 Effective Reynolds number effects on the temperature contours

The temperature contours in the annular space for various effective Reynolds number is illustrated in Fig. 9. The obtained results indicate that temperature in the annular space decreases versus Re_{eff}. In the case of smooth inner cylinder, the maximum temperature is concentrated at all the gap between the coaxial cylinders but for the

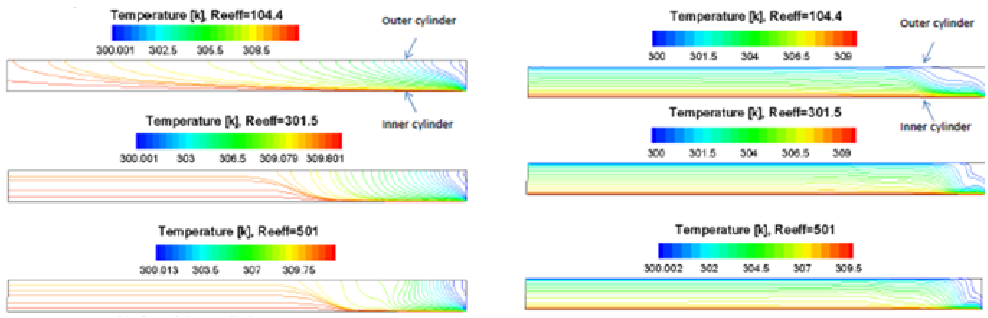

(a) (b)

Fig. 9. Development of temperature contours in the meridional plane (r, z) for: (a) smooth inner cylinder; (b) ribbed inner cylinder with 4 ribs.

ribbed inner cylinder configuration, the maximum temperature distribution is only at heated inner cylinder. This result indicates that presence of ribs on the inner cylinder contributes to enhance the cooling of the system.

4.2.3 Effective Reynolds number effects on the temperature field

The evolution of the temperature along the radial direction (at $Z = L/2$) for various effective Reynolds number is illustrated in Fig. 10. From the obtained results, it is shown that temperature decreases versus Re_{eff}. This result can be explained by the increase of mass flow rate due to increasing Re_{eff} which conducts to discharge the stored heat in the annular space.

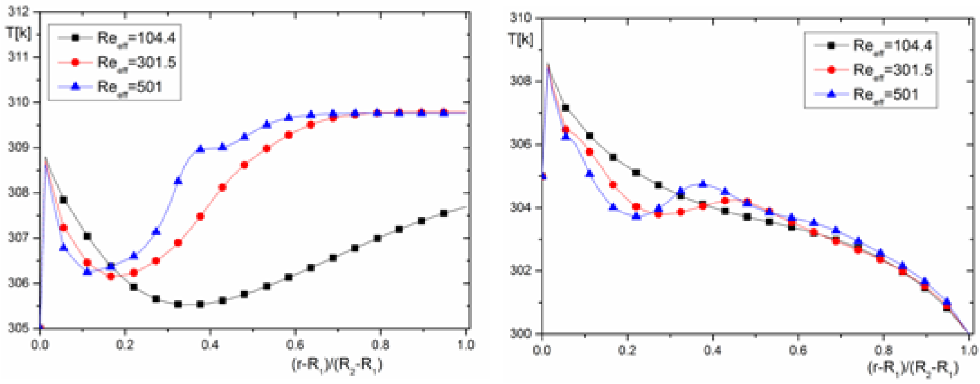

(a) (b)

Fig. 10. Evolution of the temperature along the radial position (at $Z = L/2$) for: (a) smooth inner cylinder; (b) ribbed inner cylinder with 4 ribs.

4.2.4 Effective Reynolds number effects on the average Nusselt number

Figure 11 depicts the average Nusselt number ($\overline{Nu}$) versus the effective Reynolds number (Re_{eff}) for various numbers of ribs on the inner cylinder. The analysis of the obtained results indicates that, for ribbed configuration, the $\overline{Nu}$ is improved by about 103.6% compared to smooth inner cylinder configuration for low Re_{eff} and by 312% for high Re_{eff}.

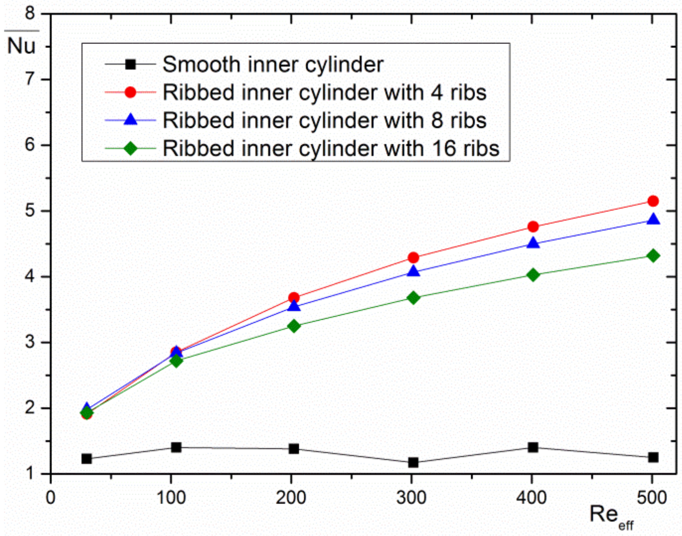

Fig. 11. Average Nusselt number ($\overline{Nu}$) versus effective Reynolds number (Re_{eff}) for various numbers of ribs on the rotating inner cylinder.

5 Conclusions

A three-dimensional numerical simulation was conducted to analyze the heat transfer characteristics of the Taylor-Couette-Poiseuille Flow (TCPF) system in the presence of ribs on the periphery of the inner cylinder. The results indicate that the combination of axial and rotational flow, along with the presence of ribs on the inner cylinder, significantly influences the heat transfer phenomenon in the annular space.

For the case of only axial flow (stationary inner cylinder), the presence of four ribs improves the average Nusselt number ($\overline{Nu}$) by approximately 65% for $Re_z = 30$ and about 29% for $Re_z = 600$. When combining axial flow with a rotating inner cylinder, the presence of four ribs enhances the average Nusselt number $\overline{Nu}$ from 103.6% at low Re_{eff} to 312% at high Re_{eff}. Furthermore, the analysis of the effect of the number of ribs (4, 8, and 16) indicates that the configuration with four ribs is the most effective for improving the cooling performance of the TCPF system.

References

[1] R.C. DiPrima (1959) The stability of viscous flow between concentric cylinders with a pressure gradient acting around the cylinders. *Journal of Fluid Mechanics* **6**(3) 462-468.

[2] S. Chandrasekhar (1961) “Hydrodynamic and hydromagnetic stability”. Oxford University Press.

[3] E.L. Koschmieder (1979) Turbulent Taylor vortex flow. *Journal of Fluid Mechanics* **93** 515-527.

[4] P.G. Drazin, W.H. Reid (1981) "Hydrodynamics stability". Cambridge Univ. Press, Cambridge.

[5] R.C. DiPrima, H.L. Swinney (1985) Instabilities and transition in flow between concentric rotating cylinders. In: H.L. Swinney, J.P. Gollub (eds) "Hydrodynamic Instabilities and the Transition to Turbulence", 2nd ed., *Topics in Applied Physics* **45**. Springer-Verlag, Berlin, pp. 139-80.

[6] G.I. Taylor (1923) Stability of a viscous liquid contained between two rotating cylinders. *Philosophical Transactions of the Royal Society of London. Series A* **223** 289-343.

[7] J.Y. Park, C.K. Choi, J.J. Kim (1994) A study on dynamic separation of silica slurry using a rotating membrane filter: 1. Experiments and filtrate fluxes. *Journal of Membrane Science* **97** 263-273.

[8] P.K. Dutta, A.K. Ray (2004) Experimental investigation of Taylor vortex photocatalytic reactor for water purification. *Chemical Engineering Science* **59** 5249-5259.

[9] P.J. Marto, L.L. Wagenseil (1979) Augmenting the condenser Heat-transfer of rotating heat pipes. *AIAA Journal* **17**(6) Art. 78-409.

[10] M. Orlowska, T. Koutchma, M. Kostrzynska, J. Tang, C. Defelice (2014) Evaluation of mixing flow conditions to inactivate Escherichia coli in opaque liquids using pilot-scale Taylor–Couette UV unit. *Journal of Food Engineering* **120** 100-109.

[11] C. Loret, W. Frith, P.J. Fryer (2007) Mechanical and structural properties of Maltodextrin/Agarose microgels composites. *Applied Rheology* **17**(3) 31412-1-31412-13.

[12] K. Ohashi, K. Toshira, F. Kushiya, T. Matsumoto, S. Yoshida, M. Endo, T. Horio, K. Ozawa, K. Sakai (1988) Rotation-induced Taylor-vortex enhances filtrate flux in plasma separation. *ASAIO Transactions* **34** 300-307.

[13] B. Haut, H. Ben Amor, L. Coulon, A. Jacquet, V. Halloin (2003) Hydrodynamic and mass transfer in a Couette-Taylor bioreactor for the culture of animal cells. *Chemical Engineering Science* **58** 777-784.

[14] J. Qiao, C.M.J. Lew, A. Karthikeyan, C. Wang (2014) Production of PEX protein from QM7 cells cultured in polymer scaffolds in a Taylor-Couette bioreactor. *Biochemical Engineering Journal* **88** 179-187.

[15] M.A. Hasoon, B.W. Martin (1977) The stability of viscous axial flow of an annulus with a rotating inner cylinder. *Proceedings of the Royal Society of London. Series A* **352** 351-380.

[16] H.A. Snyder (1962) Experiments on the Stability of Spiral Flow at Low Axial Reynolds Numbers. *Proceedings of the Royal Society of London. Series A* **265** 198.

[17] S. Lee, R.M. Lueptow (2003) Control of scale formation in reverse osmosis by membrane rotation. *Desalination* **155** 131-139.

[18] A. Daimallah, A. Bouabdallah, B. Nsom, M. Adnane, A. Alemany (2009) Onset of instabilities in Taylor-Dean flow of yield-stress fluid. *Applied Rheology* **19**(3) 33960.

[19] M. Kristiawan, M. El Hassan, A. El Faye, V. Sobolík (2019) Experimental investigation of Taylor-Couette-Poiseuille flow at low Taylor and Reynolds numbers. *PLoS ONE* **14**(4) 1-21.

[20] H. Belkadi, Y. Lagouati, V. Sobolík, H. Ouali, A. Bouabdallah (2022) Effect of axial flow on the stability of circular Couette flow. *Journal of Applied Fluid Mechanics* **15**(1) 271-281.

[21] A. Daimallah, M. Lebbi (2024) Effect of the inner cylinder endwall shape on the stability of Taylor-Couette flow. *International Journal of Applied Mechanics and Engineering* **29**(4) 96-105.

[22] T.M. Jeng, S.C. Tzeng, C.H. Lin (2007) Heat transfer enhancement of Taylor-Couette-Poiseuille flow in an annulus by mounting longitudinal ribs on the rotating inner cylinder. *International Journal of Heat and Mass Transfer* **50**(1-2) 381-390.

[23] M. Bouafia, Y. Bertin, J.B. Saulnier, P. Ropert (1998) Analyse expérimentale des transferts de chaleur en espace annulaire étroit et rainuré avec cylindre intérieur tournant. *International Journal of Heat and Mass Transfer* **41**(10) 1279-1291.

[24] S.-H. Lee, H.-T. Chung, C.-W. Park, H.-B. Kim (2009) Experimental investigation of the effect of axial wall slits on Taylor–Couette flow. *Fluid Dynamics Research* **41** 045502.

[25] Y.N. Lee, W.J. Minkowycz (1989) Heat transfer characteristics of the annulus of two-coaxial cylinders with one cylinder rotating. *International Journal of Heat and Mass Transfer* **32** 711-22.

[26] D. Liu, I.S. Kang, J.E. Cha, H.B. Kim (2010) Effect of a constant radial temperature gradient on a Taylor-Couette with axial wall slits. *Fluid Dynamics Research* **42** 065501.

[27] D. Liu, I.S. Kang, J.E. Cha, H.B. Kim (2011) Experimental study on radial temperature gradient effect of a Taylor-Couette flow with axial wall slits. *Experimental Thermal and Fluid Science 35* 1282-1292.

[28] I. Chaieb, T. Boufendi, X. Nicolas (2022) Taylor-Couette flow with mixed convection heat transfer and variable properties in a horizontal annular pipe. *Thermal Science* **26**(1A) 287-298.

[29] R. Eymard, T. Gallouët, R. Herbin (2000) Finite volume methods. *Handbook of Numerical analysis* **7** 713-1018.

[30] F.G. Carpenter (1946) Heat transfer and friction of water in an annular space. *Transactions of the American Institute of Chemical Engineers* **42** 165-187.